Finite element model of a beam structure with piezoelectric patches using RL shunt circuits

Hariri Hassan, Bernard Yves[1], Adel Razek

Paris electrical engineering laboratory, Gif sur Yvette Cedex 91192, France

Department: Modeling and control of electromagnetic systems research theme: Design control and diagnostics

Appeared in: AC2011, 14th International Conference on active systems for dynamics markets, Darmstadt, Germany, 07–08 septembre 2011,pp.124-131

1. Corresponding author; E-mail: yves.bernard@lgep.supelec.fr

Finite element model of a beam structure with piezoelectric patches using RL shunt circuits

H. Hariri, Y. Bernard, A. Razek

Laboratoire de Génie Electrique de Paris (LGEP) / SPEE-Labs, CNRS UMR 8507; SUPELEC; Université Pierre et Marie Curie P6; Université Paris-Sud 11; 11 rue Joliot Curie, Plateau de Moulon F91192 Gif sur Yvette CEDEX

Abstract

The system studied in this paper consists of a beam structure, with two non-collocated piezoelectric patches attached to its surface. One patch produces the mechanical displacement of the beam by applying an electrical voltage, while the other converts this mechanical displacement into electrical energy which is then dissipated through passive electrical networks. By using the notion of neutral axis for this asymmetric system and Hamilton principle, a finite element model, incorporating the electrical dynamics of the connected passive electrical circuits is presented. Series and parallel RL circuits are considered here. Basing on the finite element model, an iterative method to determine optimum values of the RL circuits is studied; performance comparison between series and parallel RL circuits for vibration suppression is made.

Keywords: Hamilton principle, neutral axis, finite elements model, non-collocated piezoelectric patches, RL shunted circuits, vibration suppression.

1. Introduction

The beam structures containing piezoelectric materials are used in many applications such as alignment of optical fibers [1], piezoelectric miniature robots [2], deformable mirror [3], micropumps [4], valves [5], ultrasonic motors [6] and vibration suppression [7]. To optimize these systems and to explore new applications, their numerical modeling is required. The aim of our study is to develop a finite element model to modulate a beam structure with non-collocated piezoelectric patches bonded on its surface where it is few studied in literature compared to collocated piezoelectric patches bonded on a beam structure [8-13] and then to use this model for vibration damping. Vibration damping using piezoelectric elements is also very investigated in literature [14-20]. Passive vibration damping using RL shunt circuit is chosen to study in this paper. The system studied consists in an aluminum cantilever beam actuated by a PZT patch, whose flexural vibration is transmitted to a non-collocated PZT sensor, which is connected to a series or parallel RL shunt circuits for damping the vibration (fig.1). The main point of our paper is to develop a finite element model for a beam structure with two non-collocated piezoelectric patches bonded on it and to incorporate the electrical dynamics of the connected shunt circuits. By an easy iterative way, scanning R and L

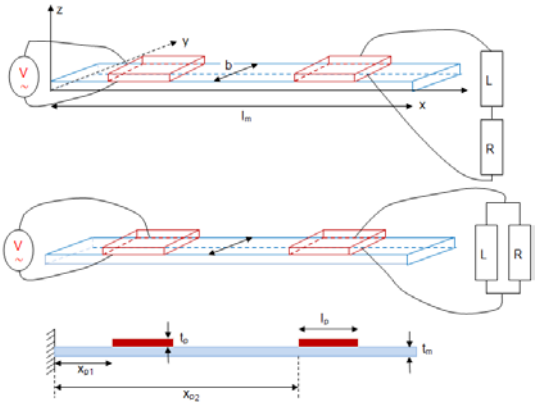

Figure 1: *Geometric parameters of the beam with non-collocated PZT actuator/sensor and RL shunt circuits bonded to sensor face*

between two boundaries, we can obtain the optimal values of R and L in series and parallel connections. Performance comparison between series and parallel RL circuits for vibration suppression is made after obtaining the RL optimal circuit. At the end of this study, conclusion and perspectives are presented.

2. Constitutive equations

The assumption of linear elastic constitutive equation of materials allows us writing the stress ten-

sor as a function of the strain tensor and vice versa.

$$\begin{cases} \{\sigma\} = [c]\{\varepsilon\} \\ \{\varepsilon\} = [s]\{\sigma\} \end{cases} \quad (1)$$

Where $\{\sigma\}$ is the stress tensor, $\{\varepsilon\}$ is the strain tensor, [s] is the elastic stiffness tensor and [c] is the compliance tensor.

Under the assumption of linear piezoelectric constitutive equations we can write

$$\begin{cases} \{\sigma\} = [c^E]\{\varepsilon\} - [\mathrm{e}]^{\mathrm{t}}\{\mathrm{E}\} \\ \{D\} = [\mathrm{e}]\{\varepsilon\} + [\epsilon^{\varepsilon}]\{\mathrm{E}\} \end{cases} \quad (2)$$

Where [e] is the piezoelectric coefficient tensor, $[\epsilon^{\varepsilon}]$ is the dielectric permittivity at constant strain condition and $[c^E]$ is the elastic stiffness tensor at constant electric field.

3. Model hypothesis

We define a displacement field vector by the displacement of a point M(x,y,z) of the system to M' at instant t.

$$\mathrm{MM'(x,y,z,t)} = \{\mathrm{u}\} = \begin{cases} u_1(x,y,z,t) \\ u_2(x,y,z,t) \\ u_3(x,y,z,t) \end{cases} \quad (3)$$

Where u_i is the displacement along i-axis. We consider this displacement field as the unknown must be determined to know the status of the system at all times.

Equations of the system are derived based on the following assumptions:

1. Euler-Bernoulli hypothesis i.e. uniaxial stress in the x-direction, small deformation and cross section remain perpendicular to the neutral axis after deformation.
2. The electric field is assumed to be uniformly distributed in the z-direction $\{\mathrm{E}\} = \mathrm{E}_3(\mathrm{x,t})$
3. The poling direction of the piezoelectric layer is in the positive z-direction
4. Perfect bonding between the piezoelectric layer and the aluminium layer
5. No external forces are applied to the system

Then, the displacement field becomes

$$\{\mathrm{u}\} = \begin{cases} u_1(x,y,z,t) \approx -(z-z_n)\,\partial_x w \\ u_2(x,y,z,t) = 0 \\ u_3(x,y,z,t) \approx w(x,t) \end{cases} \quad (4)$$

Where $w(x,t)$ is the transverse displacement of the neutral axis of the system z_n. z_n can be calculated by setting to zero the sum of all forces in x-direction over the entire cross-section [21], here z_n is computed from the bottom of the system according to the coordinate system taken in figure 1:

$$\mathrm{b}\int_0^{t_m} \sigma_1^m(z)dz + \mathrm{b}\int_{t_m}^{t_m+t_p} \sigma_1^p(z)dz = 0 \quad (5)$$

Where σ_1^p and σ_1^m are referred to as stresses induced in the piezoelectric and aluminium layers in x-direction. According to uniaxial stress assumption, we can write

$$\sigma_1^m = \mathrm{c_m}\,\varepsilon_1 ,$$

$$\sigma_1^p = \mathrm{c_p}\,\varepsilon_1 - \mathrm{e_p}E_3 = \frac{1}{s_{11}^E}\varepsilon_1 - \frac{d_{31}}{s_{11}^E}E_3 ,$$

$$D_3 = \mathrm{e_p}\,\varepsilon_1 + \epsilon_p^{\varepsilon}\,E_3 = \frac{d_{31}}{s_{11}^E}\varepsilon_1 + \left(\varepsilon_{33}^{\sigma} - \frac{d_{31}^2}{s_{11}^E}\right)E_3 \quad (6)$$

Where $[c^E] = \mathrm{c_p} = \frac{1}{s_{11}^E}$ is the Young modulus for the piezoelectric layer, $[\mathrm{e}] = \mathrm{e_p} = \frac{d_{31}}{s_{11}^E}$ is the piezoelectric constant, $[\mathrm{c}] = \mathrm{c_m}$ is the Young modulus for the aluminum layer, s_{11}^E is the elastic compliance for the piezoelectric layer at constant electric field, d_{31} is the piezoelectric constant and $[\epsilon^{\varepsilon}] = \epsilon_p^{\varepsilon} = \varepsilon_{33}^{\sigma} - \frac{d_{31}^2}{s_{11}^E}$ where $\varepsilon_{33}^{\sigma}$ is the electrical permittivity at constant stress for the piezoelectric layer. Properties and geometric parameters for the PZT and aluminium layers are given in table 1. ε_1 is the strain in the x-direction and is defined by

$$\{\varepsilon\} = \varepsilon_1 = \partial_x u_1 = -(z-z_n)\,\partial^2{}_x w \quad (7)$$

Utilizing Hook's law, while substituting strain relationship from (5), yields:

$$\int_0^{t_m} c_m(z-z_n)dz + \int_{t_m}^{t_m+t_p} c_p(z-z_n)\,dz = 0 \quad (8)$$

Upon simplifying, the neutral axis $\mathrm{z_n}$ can be obtained as shown in equation (9) at the end of the paper.

4. Variational equation

Hamilton principle is the most widely used one for dynamic structures [7]. All variations at each known instant are zero.

$$\delta\int_{t_1}^{t_2}(\mathcal{L} + W)\mathrm{dt} = 0 \quad (10)$$

Where $\mathcal{L}$ is the Lagrangian ($\mathcal{L}$ = J - H with J the kinetic energy and H the global enthalpy) and

W is the virtual work of external mechanical and

Properties/materials	PZT	Aluminum
Young's modulus (Pa)	-	$c_m = 69 \times 10^9$
Poison's ratio	-	$\upsilon_m = 0.33$
Volume density ($Kg.m^3$)	$\rho_p = 7900$	$\rho_m = 2700$
Relative permittivity	$\varepsilon_{33r}^{\sigma} = 1282.1$	-
Piezoelectric constant ($m.V^{-1}$)	$d_{31} = -1.3e^{-10}$	-
Elastic compliances (Pa^{-1})	$s_{11}^{E} = 1.3e^{-11}$	-
Length(l) ×width(b) × thickness$(t_p$ & $t_m)$ (mm^3)	32×17×0.27	180×17×0.5

Table 1: *properties and geometric parameters for the PZT and aluminum layers*

electric forces. The kinetic energy is equal to (ρ is the volume density)

$$J=\int_V \frac{1}{2}\rho \{\dot{u}\}^t\{\dot{u}\}dV \quad (11)$$

The global enthalpy is equal to

$$H = \int_V \frac{1}{2}(\{\varepsilon\}^t\{\sigma\} - \{E\}^t\{D\})dV \quad (12)$$

And finally, the virtual work of external mechanical and electrical forces is equal to

$$W = \int_V \{u\}^t \{F_V\}dV + t_p\{E\}Q \quad (13)$$

Where $\{F_V\}$ represents the body applied forces, t_p the thickness of piezoelectric layer, Q the electric charge.

By replacing $\{\sigma\}$ and {D} by their equation (2) in (12), integrating by parts the kinetic energy (11) and applying Hamilton principle, the variational equation is obtained in (14).

$$\text{Where } \{\delta u\} = \begin{cases} -(z-z_n)\,\partial_x \delta w \\ 0 \\ \delta w(x,t) \end{cases} \quad (15)$$

$$\{\delta\varepsilon\} = \delta\varepsilon_1 = -(z-z_n)\,\partial^2{}_x \delta w \quad (16)$$

Integrating equation (14) over the entire volume of the system, we obtain the equation (17). Where $E_{3p1}(t)$,$E_{3p2}(t)$,$\in_p$, Q_{p1} and Q_{p2} are the electric fields, dielectric permittivity and electric charges for the two piezoelectric patches.

5. Finite element model

Using Hermite element as mentioned in [7] to write the solution w(x,t) as function of the corresponding node values w_i and the shape function $[\lambda]$. At each node, the unknowns are w_i and $\partial_x w_i$ to ensure C^1 continuity. So, one element (two nodes) is linked to four unknowns and four shape functions. Then, we integrate equation (17) over each element along the beam length to obtain the elementary matrices. To obtain the assembly matrices of the system, we must assemble the elementary matrices obtained by integration over each segment; taking into account the equality of node values of an element with its neighbouring ones. Boundary conditions are taken into account also during the assembly of matrices. Finally, we obtain the FE model of the system as shown in equation (23). Where [M] is the mass matrix and [K] is the stiffness matrix. A damping matrix [C] determined experimentally [22] is integrated in the system via Rayleigh damping to match the damping behavior of the real system. And the model of the system is represented in equation (24).

6. RL shunt circuits

At this point a finite element model of the system is determined. We consider know that the piezoelectric patch number two (p2) is connected to an electrical RL shunt circuit as shown in figure 1. Then, we can write

$$E_{3p2}t_p = z_e\dot{Q}_{p2} \quad (25)$$

Where z_e is the electrical impedance of the series or parallel RL circuit and is written as

$$z_e = \begin{cases} jwL + R \;\; (series) \\ \frac{jwLR}{jwL+R} \;\; (parallel) \end{cases} \quad (26)$$

Where w is the frequency of the applied electric field E_{3p1}, L and R are the inductance and the resistance of the electrical circuit connected to the piezoelectric patch number two (p2).

To incorporate the series or parallel RL shunt circuits in the model, otherwise z_e, it is useful to appear $\dot{Q}_{p2}$ in the matrix equation (24), i.e to take it as an unknown. So, mass matrix will be the same, damping and stiffness matrix will change as shown in equation (27).

After incorporating the electrical circuit in the model, three electrical impedances (R, RL series & RL parallel) were connected to the piezoelectric patch p2. These kinds of circuits are known in the literature by the single mode damping [22]

because they are able to suppress the vibration for one single frequency i.e. for each frequency there are an optimal electric circuit. We take here, the fourth resonant mode of vibration at frequency f_4= 484.3 Hz to determine optimal values of the electrical circuits. The process stills the same for any other frequency.

Let us beginning with the first electrical circuit where a resistance is connected to p2. By scanning the resistance and calculating the displacement using the finite element model for each resistance, we can find the optimal value of resistance corresponding to a minimum displacement of the beam. Figure 2, shows the optimal resistance obtained using our finite element model and it is equal to 15 KΩ. It is noted in simulation that, for any resonant frequency taken, the optimal resistance value is approximately equal to the value obtained in the formula of equation (28).

$$R_{opt} = \frac{1}{2\pi f_r C_p} \qquad (28)$$

Where f_r is the resonance frequency and C_p is the electrical capacitance of the PZT sensor and can be calculated using table 2.

	Simulation	Formula
C_p	$\frac{K_{vvp2}}{t_p^2}$	$\frac{\varepsilon_{33r}^T \varepsilon_0 l_p b}{t_p}$
C_p(nF)	20	22

Table 2: Comparison between simulation and theory for the capacitance value obtained

The graph at the top of figure 2 shows the tip displacement of the beam function of resistance at the fourth resonant frequency and the graph at the bottom shows displacement versus frequency around the fourth resonant one, for three different values of resistance. Figure 2, can be shown that the damping suppression is not very sensitive for resistance shunt circuit.

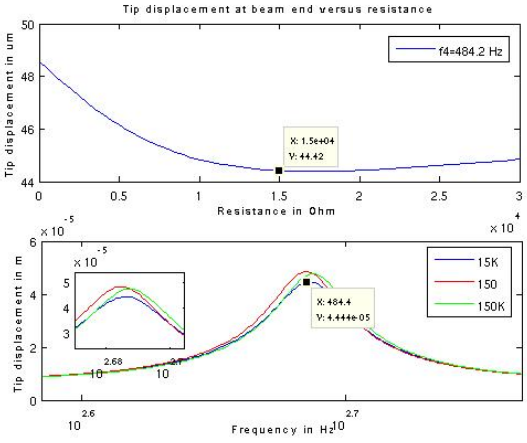

Figure 2: *Optimal resistance for damping suppression in the case of resistance shunt circuit*

In case of RL shunt circuit connected to p2, there are two parameters (R & L) to be varied to get the minimum displacement of the beam. Let us starting by fixing the resistance to the optimal value obtained by resistance shunt circuit and, varied the inductance to get the optimal value. Figure 3, shows the optimal inductance at fixed R=15 KΩ for parallel and series connections. The obtained

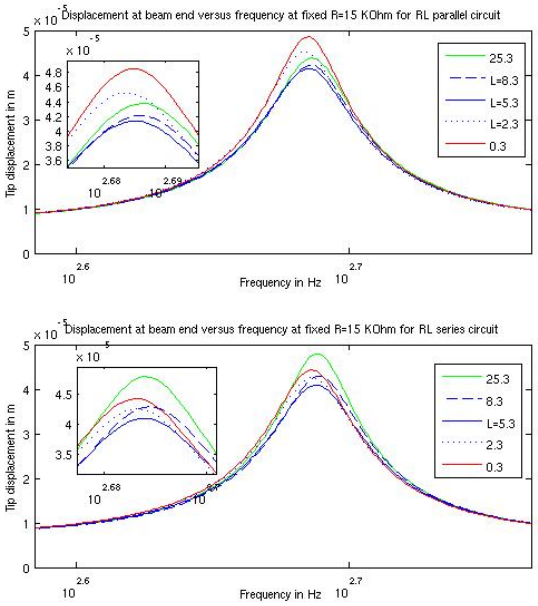

Figure 3: *Optimal inductance in H at fixed R value for parallel and series connections.*

value of L is equal to the inductance tuning the shunt effect to the frequency of the disturbance, according to (29).

$$L_{opt} = \frac{1}{(2\pi f_r)^2 C_p} \qquad (29)$$

It is noted in simulation that, for any resonant frequency taken, the optimal inductance is always verifying equation (29).

According to equation (26), in series connection, for small values of R compared to jwL, the impedance behaves like an inductor and, for large values of R compared to jwL, the influence of L is not considered. In parallel connection, for small values of R compared to jwL, L is not considered and for large values of R compared to jwL, L dominates. We can notice by simulation that, for any R values between these two extremes, the optimal inductance is still verify equation (29) and it is independent of R values in series and parallel connections. Wu [23] demonstrated that for series RL shunt, the optimal inductance is dependant of R values in case of large R. As mentioned before, there is no influence of L to the

system displacement in case of large R values and, the electric circuit can be considered as a resistance shunt. Being given the optimal inductance (5.3 H) verifying equation (29), scanning R values to find the optimal one. Figure 4 & 5; show the tip displacement versus frequency for different R values. Figure 4, shows that, for large R values the tip displacement is approximately equal to that obtained in figure 2, when resistance shunt circuit is used. And for small R values, the system behavior corresponds to an inductance only. Less than 4 KΩ, the system behavior becomes slightly inductance. Inversely in the case of parallel connection, the tip displacement is approximately equal to that obtained in figure 2, for small R values and inductance behavior for large R values. 75 KΩ can be chosen as an optimal R value.

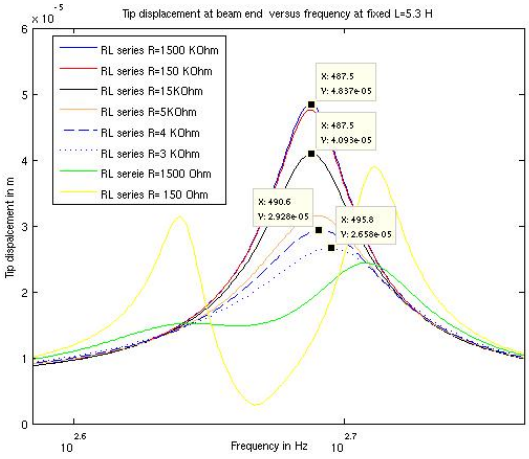

Figure 4: *Optimal R value for series connection.*

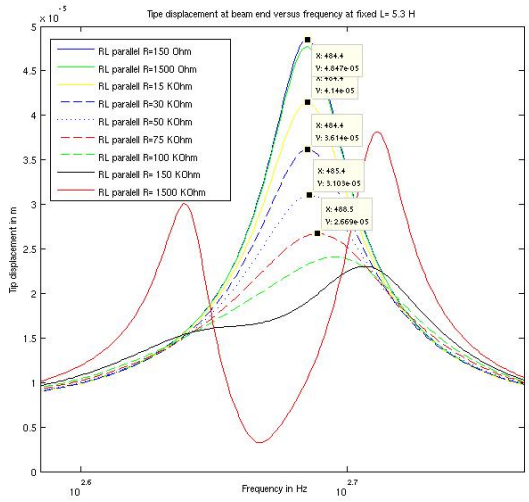

Figure 5: *Optimal R value for parallel connection.*

Rebuild figure 3 at optimal R values as shown figure 6. It was expected to obtain the same optimal inductance with a smaller displacement. Figure 7 shows displacement comparison between open circuit, optimal resistance shunt circuit, optimal RL shunt circuit in both series and parallel connections. The vibration suppression performance is evaluated based on amplitude of the displacement. The best performance is obtained for minimal displacement. According to figure 7, the optimal RL parallel shunt circuit shows a performance slightly better than the RL series shunt circuit.

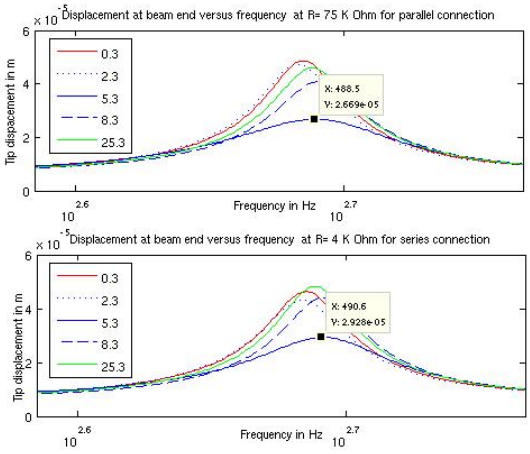

Figure 6: *Optimal inductance in H at optimal R value for parallel and series connections*

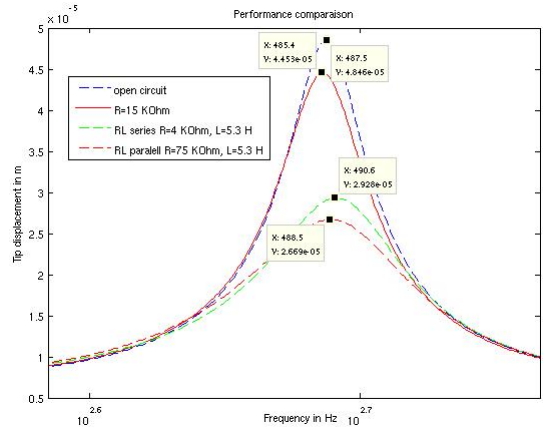

Figure 7: *Performance comparison between shunt circuits*

7. Conclusion

Our paper is the first one in the literature that studied the damping vibration for non-collocated piezoelectric patches bonded on a thin beam structure in the configuration presented in figure 1. In this paper we developed a finite element model of the system and then, we incorporate the electrical dynamics of the connected passive electrical circuits. Optimal values for the shunt circuits are determined by an iterative method using the finite element model.

The model studied, including the passive electrical network must be verified experimentally in future work and this new configuration of system

used for damping application must be compared in term of performance with the other existing one. The finite element model developed here will be taken as support to study a non-collocated piezoelectric patches bonded on a plate, for the same type of applications.

$$\begin{cases} \frac{1}{2}\,\frac{c_m t_m{}^2 + c_p t_p{}^2 + 2c_p t_p t_m}{c_m t_m + c_p t_p} & if\ x_{p1} < x < x_{p1} + l_p\ et\ x_{p2} < x < x_{p2} + l_p \\ \frac{t_m}{2} & if\ not \end{cases} \quad (9)$$

$$\int_V (-\rho\{\delta u\}^t\{\ddot{u}\} - \{\delta\varepsilon\}^t[c]\{\varepsilon\} + \{\delta\varepsilon\}^t[e]^t\{E\} + \{\delta E\}^t[e]\{\varepsilon\} + \{\delta E\}^t[\epsilon^\varepsilon]\{E\} + \{\delta u\}^t\{F_v\})dV +$$

$$t_p\{\delta E\}Q = 0 \quad (14)$$

$$\int_0^{x_{p1}} A(x,t)dx + \int_{x_{p1}}^{x_{p1}+l_p}[B(x,t) + qe_pE_{3p1}(t)\partial^2{}_x\delta w + \delta E_{3p1}(t)qe_p\partial^2{}_x w]dx +$$
$$\int_{x_{p1}+l_p}^{x_{p2}} A(x,t)dx + \int_{x_{p2}}^{x_{p2}+l_p}[B(x,t) + qe_pE_{3p2}(t)\partial^2{}_x\delta w + \delta E_{3p2}(t)qe_p\partial^2{}_x w]dx + \int_{x_{p2}+l_p}^{l} A(x,t)dx -$$
$$\delta E_{3p1}(t)\, l_p b t_p \in_p E_{3p1}(t) - \delta E_{3p2}(t)\, l_p b t_p \in_p E_{3p2}(t) - t_p\delta E_{3p1}(t)Q_{p1} - t_p\delta E_{3p2}(t)Q_{p2} - {}^t\{\delta u\}\{F\} = 0$$

(17)

Where

$$A(x,t) = \rho_m I_m \partial_x\delta w.\ \partial^2{}_t(\partial_x w) + b\rho_m t_m\ \delta w.\ \partial^2{}_t w + I_m c_m\ \partial^2{}_x\delta w.\ \partial^2{}_x w \quad (18)$$

$$B(x,t) = (\rho_p I_p + \rho_m I_m)\partial_x\delta w.\ \partial^2{}_t(\partial_x w) + b(\rho_p t_p + \rho_m t_m)\ \delta w.\ \partial^2{}_t w + (I_p c_p + I_m c_m)\ \partial^2{}_x\delta w.\ \partial^2{}_x w \quad (19)$$

$$I_m = b\int_0^{t_m}(z - z_n)^2\,dz = b\,\frac{1}{3}\,[(t_m - z_n)^3 + z_n{}^3] \quad (20)$$

$$I_p = b\int_{t_m}^{t_p+t_m}(z - z_n)^2\,dz = b\,\frac{1}{3}\,[(t_p + t_m - z_n)^3 - (t_m - z_n)^3] \quad (21)$$

$$q = b\int_{t_m}^{t_p+t_m}(z - z_n)\,dz = b\,\frac{1}{2}\,[(t_p + t_m - z_n)^2 - (t_m - z_n)^2] \quad (22)$$

$$\begin{bmatrix} M & 0 & 0 \\ 0 & 0 & 0 \\ 0 & 0 & 0 \end{bmatrix}\begin{bmatrix} \ddot{U}_i \\ \ddot{E}_{3p1} \\ \ddot{E}_{3p2} \end{bmatrix} + \begin{bmatrix} K_{mm} & K_{mvp1} & K_{mvp2} \\ K_{vmp1} & K_{vvp1} & 0 \\ K_{vmp2} & 0 & K_{vvp2} \end{bmatrix}\begin{bmatrix} U_i \\ E_{3p1} \\ E_{3p2} \end{bmatrix} = \begin{bmatrix} F_i \\ t_pQ_{p1} \\ t_pQ_{p2} \end{bmatrix} \quad (23)$$

$$\begin{bmatrix} M & 0 & 0 \\ 0 & 0 & 0 \\ 0 & 0 & 0 \end{bmatrix}\begin{bmatrix} \ddot{U}_i \\ \ddot{E}_{3p1} \\ \ddot{E}_{3p2} \end{bmatrix} + \begin{bmatrix} C & 0 & 0 \\ 0 & 0 & 0 \\ 0 & 0 & 0 \end{bmatrix}\begin{bmatrix} \dot{U}_i \\ \dot{E}_{3p1} \\ \dot{E}_{3p2} \end{bmatrix} + \begin{bmatrix} K_{mm} & K_{mvp1} & K_{mvp2} \\ K_{vmp1} & K_{vvp1} & 0 \\ K_{vmp2} & 0 & K_{vvp2} \end{bmatrix}\begin{bmatrix} U_i \\ E_{3p1} \\ E_{3p2} \end{bmatrix} = \begin{bmatrix} F_i \\ t_pQ_{p1} \\ t_pQ_{p2} \end{bmatrix} \quad (24)$$

$$\begin{bmatrix} M & 0 & 0 \\ 0 & 0 & 0 \\ 0 & 0 & 0 \end{bmatrix}\begin{bmatrix} \ddot{U}_i \\ t_p\ddot{Q}_{p1} \\ t_p\ddot{Q}_{p2} \end{bmatrix} + \begin{bmatrix} C & 0 & 0 \\ 0 & 0 & 0 \\ 0 & 0 & -\frac{z_e}{t_p^2} \end{bmatrix}\begin{bmatrix} \dot{U}_i \\ t_p\dot{Q}_{p1} \\ t_p\dot{Q}_{p2} \end{bmatrix} +$$

$$\begin{bmatrix} K_{mm} - K_{mvp1}K_{vvp1}^{-1}K_{vmp1} - K_{mvp2}K_{vvp2}^{-1}K_{vmp2} & K_{mvp1}K_{vvp1}^{-1} & K_{mvp2}K_{vvp2}^{-1} \\ -K_{vvp1}^{-1}K_{vmp1} & K_{vvp1}^{-1} & 0 \\ -K_{vvp2}^{-1}K_{vmp2} & 0 & K_{vvp2}^{-1} \end{bmatrix}\begin{bmatrix} U_i \\ t_pQ_{p1} \\ t_pQ_{p2} \end{bmatrix} = \begin{bmatrix} F_i \\ E_{3p1} \\ 0 \end{bmatrix} \quad (27)$$

References

[1] A. Tuominen, J. Lappalainen , J. Hiltunen ,J. Ollila and V. Lantto, “Piezoelectric thin-film unimorph actuator for optical fibre alignment applications”, Journal of optics a: pure and applied optics 8, 2006.

[2] K. J. Son, V. Kartik, J. A. Wickert and M. Sitti, “ An ultrasonic standing-wave-actuated nano-positioning walking robot: Piezoelectric-metal composite beam modeling”, Journal of vibration and control, Vol. 12, no. 12, pp. 1293-1309, 2006.

[3] Y. Hishinuma and E.H. Yang, “Pizoelectric unimorph microactuator arrays for single-crystal silicon continuous-membrane deformable mirror” Journal of microelectromechanical systems,Vol. 15, no. 2, April 2006.

[4] D. Accoto, M. C. Carrozza and P. Dario, “Modelling of micropumps using unimorph piezoelectric actuator and ball valves”, Journal of Micromechanics and Microengineering, Vol.10, no. 2, March 2000.

[5] M. Sobocinski, J. Juuti, H. Jantunen, L. Golonka, “Piezoelectric unimorph valve assembled on an LTCC substrate”, Sensors and Actuators A 149, pp.315–319, 2009.

[6] W H Duan, S T Quek and Q Wang, ‘’A novel ring type ultrasonic motor with multiple wavenumbers: design, fabrication and caracterisation’’, Jornal of smart materials and structures 18, 2009.

[7] Romain Corcolle, Erwan Salaün, Frédéric Bouillault, Yves Bernard, Claude Richard, Adrien Badel, Daniel Guyomar "Modeling of a beam structure with piezoelectric materials:introduction to SSD techniques", COMPEL: The International Journal for Computation and Mathematics in Electrical and Electronic Engineering, Vol.27 Issue: 1, pp.205 – 214, 2008.

[8] C.H. Nguyen, S.J. Pietrzko, ‘’ FE analysis of a PZT- actuated adaptive beam with vibration damping using a parallel R-L shunt circuit’’, journal of finite elements in analysis and design 42, pp. 1231-1239, 2006.

[9] C.H. Park, 44 Dynamics modelling of beams with shunted piezoelectric elements’’, Journal of Sound and vibration 268, pp. 115-129, 2003.

[10] S.Y. Wang, S.T. Quek, K.K. Ang, ‘’Dynamic stability analysis of finite element modelling of piezoelectric composite plates’’, International journal of solids and vibrations 41, pp. 745-764, 2004.

[11] V. V. Varadan, ‘’ closed loop finite element modelling of active/passive damping in structural vibration control’’, Journal of smart materials and structures 5, pp. 685-694, 1996.

[12] G.L.C.M. de Abreu, J.F. Ribeiro and V. Steffen, ’’ Finite element modelling of a plate with localized piezoelectric sensors and actuators’’ Journal of the Braz. Soc. of Mech. Sci. & Eng., Vol. 26, No. 2, April-June 2004.

[13] M. Y. Yasin, N. Ahmad, M. N. Alam, ‘’ Finite element analysis of actively controlled smart plate with patched actuators and sensors’’, Latin American journal of solids and structures 7, pp. 227-247, 2010.

[14] R. Corcolle, Fréderic Bouillaut, Y. Bernard, ‘’ Modeling of a plate structure with piezoelectric patches: Damping applicatin ‘’, IEEE transaction on magnetics, vol. 44,No. 6, June 2008.

[15] C. C. Lin, H. N. Huang, ‘’ Vibration control of beam-plates with bonded piezoelectric sensors and actuators’’, Computers and structures 73, pp. 239-248, 1999.

[16] W W Law, W-H Liao, J Huang,’’ Vibration control of structures with self sensing piezoelectric actuators incorporating adaptive mechanisms’’, Smart mater. Struct. 12, pp. 720-730, 2003.

[17] M A Foda, A A almajed , M M Elmadany, ‘’ Vibration suppression of composite laminated beams using distributed piezoelectric patches’’, Smart Mater. Struct. 19, 2010.

[18] J. Becker, O. Fein, M. Maess, L. Gaul, ‘’Finite element-based analysis of shunted piezoelectric structures for vibration damping’’, Computers and structures 84, pp. 2340-2350, 2006.

[19] K. Yamada, H. Matsuhisa, H. Utsuno, K. Sawada, ‘’ Optimum tuning of series and parallel LR circuits for passive vibration using piezoelectric elements’’, Journal of sound and vibration 329, pp. 5036-5057, 2010.

[20] C.H. Nguyen, S.J. Pietrzko, ‘’ FE analysis of a PZT-actuated adaptive beam with vibration damping using a parallel R-L shunt circuit’’, Finite Elements in analysis and design 42, pp. 1231-1239, 2006.

[21] R.G. Ballas, “piezoelectric multilayer beam bending actuator”, Springer, 2007.

[22] S.O. Reza Moheimani and Andrew J. Fleming, ‘’ Piezoelectric Transducers for Vibration Control and Damping’’, Springer 2006.

[23] S. Y. Wu, “Piezoelectric shunts with parallel R-L circuit for smart structural damping and vibration control,” in Proc. SPIE Symp. Smart Structures Materials Passive Damping Isolation, , pp. 259–269, Mar. 1996.